Mapping hydrothermally altered rocks with Landsat 8 imagery: A case study in the KSM and Snowfield zones, northwestern British Columbia

Tian Han[1, a] and JoAnne Nelson[1]

[1] British Columbia Geological Survey, Ministry of Energy and Mines, Victoria, BC, V8W 9N3
[a] corresponding author: Tian.Han@gov.bc.ca

Abstract

Mapping hydrothermally altered rocks, which are common indicators of mineralization, is integral to reconnaissance mineral exploration. Multi-spectral moderate-resolution satellite remote sensing has long-been applied to map altered rocks, offering wide spatial coverage, low cost, and simple image analysis. Most previous studies have been in un-vegetated arid or semi-arid areas. Use of this technique in much of the Canadian Cordillera faces the challenge of extensive cover by vegetation, ice, snow, and water along with high relief. We use Landsat 8 imagery, generated in August, 2013, of the Iskut region in northwestern British Columbia, a recently deglaciated area with abundant porphyry copper-related gossans, to develop a regional map depicting hydrothermal alteration. Integrated with ground observations of rock type, alteration, vegetation, and overburden at 100 field sites, traditional spectral unmixing image analysis was only partly successful in discriminating the spectral responses of altered and unaltered rocks. However, screening for the influence of topography (slope and aspect) was more successful. Our image-derived alteration map matched observations at 83% of the field sites. Altered rocks were unrecognized by spectral unmixing at 17% of the field sites, likely reflecting weak alteration or limited exposure of altered rocks. Based on these preliminary results, spectral unmixing of Landsat-8 images that account for high-relief topography is a potential tool to identify alteration haloes in less well known mineralized areas of British Columbia.

Keywords: Hydrothermal alteration mapping, remote sensing, Landsat 8, spectral unmixing, altered rock, image analysis, topography
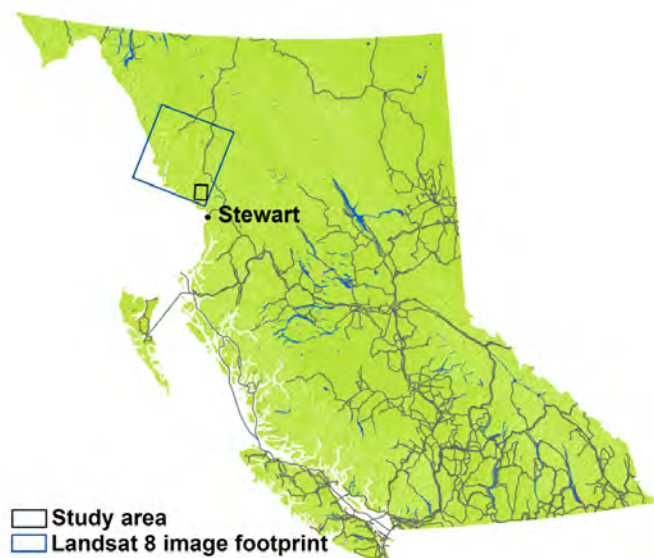
1. Introduction

Given the common proximity of hydrothermally altered rocks to mineral deposits, regional mapping of exposed altered rocks by remote sensing has proven a useful complement to field exploration (Sabins, 1999). Multi-spectral moderate-resolution satellite remote sensing imagery, such as offered by NASA's Landsat satellites, has been used for regional mineral exploration since the early 1970s, which culminated in 1999 with the operation of ASTER (Advanced Space-borne Thermal Emission and Reflection Radiometer) onboard NASA's Terra satellite. A number of studies have demonstrated the utility of these data in geological mapping. Rowan et al. (1974) working in Goldfield, Nevada developed band-ratio and color-composite methods to enhance visibility of hydrothermally altered rocks, methods that have become the standard approach for geological applications. Loughlin (1991) analyzed Landsat Thematic Mapper (TM) images near the Gold Bar deposit in Nevada, generating a map highlighting hydrothermal alteration assemblages, including hydroxyl-bearing and iron-oxide minerals. Mars and Lawrence (2006) used ASTER images to map argillic- and phyllic-altered rocks near porphyry copper deposits in the Zagros magmatic arc of Iran. Gabr et al. (2010) used ASTER images from Abu-Marawat (Egypt) to separate mineralized and un-mineralized rocks based on abundance of secondary iron-oxide minerals.

Although extensively altered rocks can be identified visually using colour aerial photographs or high-resolution images, multi-spectral moderate-resolution satellite images: 1) provide broad spatial coverage, yielding a synoptic view across entire hydrothermal systems; 2) capture both visible and shortwave infrared spectra (where many mineral-related absorption features reside; van der Meer, 2004); 3) can generally be obtained at no cost; and 4) can be quantitatively analyzed at a regional scale. In the summer of 2013, the United States Geological Survey (USGS) released images acquired by the Operational Land Imager (OLI) and Thermal Infrared Scanner (TIRS) onboard the Landsat 8 satellite, which was launched by NASA earlier in the year. The Landsat-8 images are enhanced relative to previous generations by the addition of aerosol and cirrus bands (Table 1), improved signal-to-noise ratios using a pushbroom imager, and high-radiometric resolution that uses 12-bit quantization. These enhancements hold promise for geological applications, including alteration mapping.

The present study is the first attempt to use Landsat 8 OLI and TIRS images to map hydrothermally altered rocks in the Cordillera of British Columbia. Hitherto, Landsat-based alteration mapping studies have mainly focused on arid or semi-arid areas with abundant un-vegetated bedrock exposures (e.g., Rowan et al., 1974; Loughlin, 1991; Mars and Lawrence, 2006; Gabr et al., 2010). Extensive cover by vegetation, snow, ice, and water bodies, along with high relief pose problems for alteration mapping based on analyzing multi-spectral moderate-resolution images across much of the Canadian Cordillera. Our study examines the area near the Kerr-Sulphurets-Mitchell (KSM) and Snowfield zones in northwestern British Columbia (Fig. 1), where recent deglaciation has created broad exposures

103

Geological Fieldwork 2014, British Columbia Ministry of Energy and Mines, British Columbia Geological Survey Paper 2015-1

Fig. 1. Location of study areas and area covered by Landsat 8 image.

of bedrock, including alteration zones. Herein we describe steps to streamline image processing and analysis and to integrate ground observations with satellite imagery. We use spectral unmixing image analysis to distinguish altered rocks from unaltered rocks and other substances and to produce a map outlining the regional distribution of hydrothermal alteration.

2. Study area and ground observations

The Kerr-Sulphurets-Mitchell (KSM) and Snowfield zones are approximately 60 kilometres north of the town of Stewart, in northwestern British Columbia (Figs. 1, 2). In this region, porphyry-style systems are expressed as extensive gossans (Fig. 3). Recent deglaciation has resulted in widespread bedrock and colluvial exposures, creating a natural laboratory to compare outcrop geology and satellite imagery. Fieldwork was conducted in the summer of 2013 during regional bedrock

mapping (Nelson and Kyba, 2014). Detailed observations were made in four areas, near the Bruce and Treaty glaciers, and in the Iron Cap and Snowfield alteration zones (Fig. 2). Most outcrops near Bruce and Treaty glaciers are of unaltered rock, in many cases partly covered with lichen, moss, heather, and sedge grasses, and thin Quaternary gravels. These outcrops were used as standards to compare with the intensely altered rocks of the Iron Cap and Snowfield gossans. Iron Cap displays potassic, phyllic and silica-clay-sericite alteration, whereas Snowfield displays quartz-sericite-pyrite-clay and advanced argillic assemblages. Different alteration assemblages create outcrops of different morphology. For instance, silica-pyrite alteration produces resistant cliff outcrops, whereas clay-rich alteration assemblages result in extensive colluvium.

Ground observation sites (Fig. 2) were selected to represent the diversity of rock surfaces in terms of alteration, exposure, slope, and aspect, all of which influence spectral responses captured by satellite sensing instruments. Most of the sites have an area of 900 m^2 or more, large enough to be captured as a single pixel (30 m x 30 m) on the Landsat 8 OLI image. Site locations were established using hand-held GPS (with a ~3 m accuracy). After the fieldwork, we created a reference library that combines ground observations with spectra derived from the Landsat 8 image in a spatial database (Fig. 4) for current and future remote sensing mapping.

3. Landsat 8 image and preprocessing

Landsat 8 is equipped with the Operational Land Imager (OLI) and the Thermal Infrared Sensor (TIRS), which are able to collect up to 550 multispectral images daily (Irons et al., 2012; USGS, 2013a). Each image covers an area with dimensions of 170 km (north-south) by 183 km (east-west). Landsat 8 images, available to the public since July 2013, can be downloaded from several USGS websites, including the Earth Explorer (USGS, 2013b). The images are available at different processing levels (referred to as products). In the Level 1T product, used in the current study, raw images were

Table 1. Landsat 8 instrument bands.

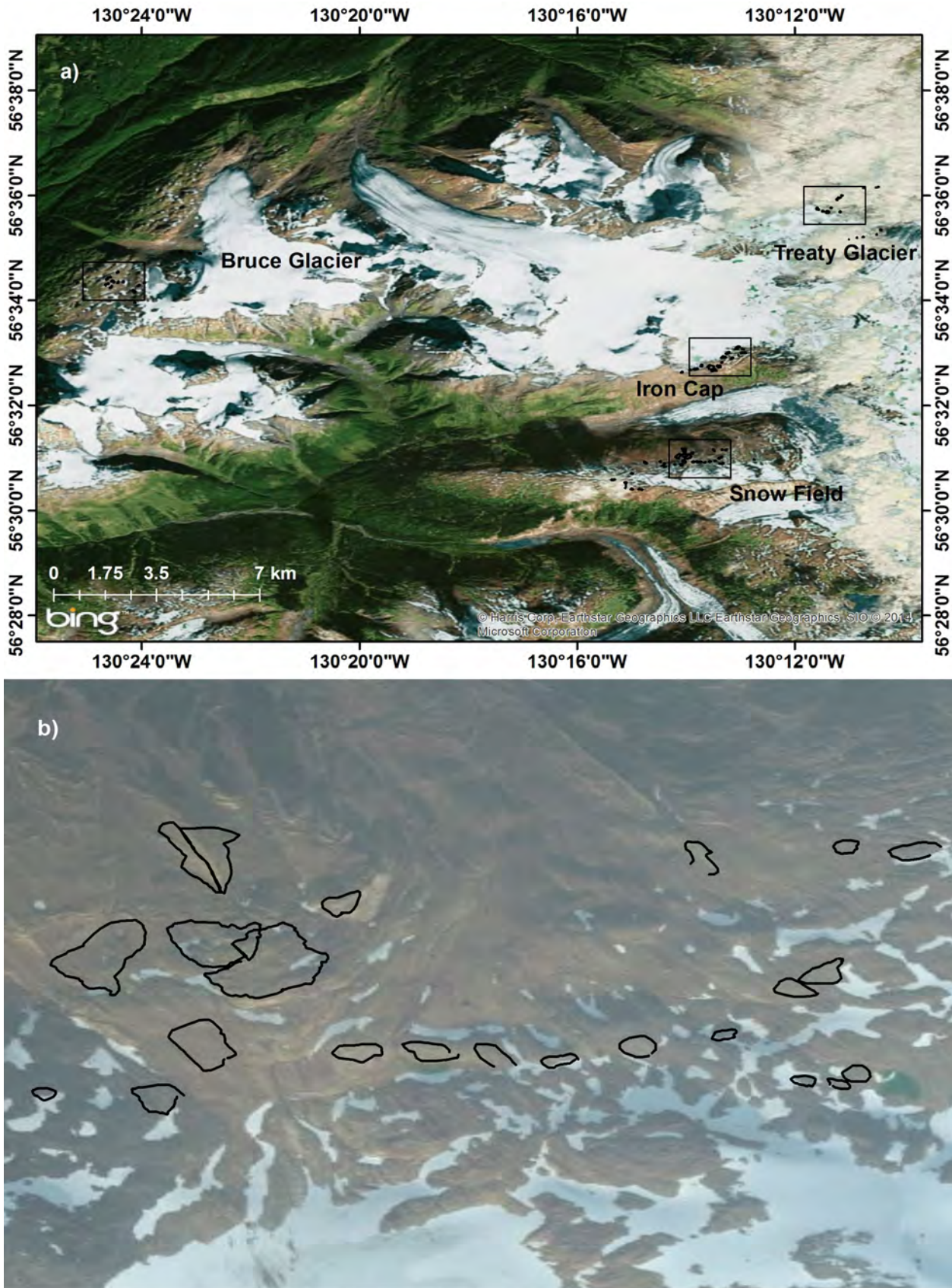| Band #	Band name	Wavelength (μm)	Spatial resolution (m)
1	Coastal aerosol	0.43 - 0.45	30
2	Blue	0.45 - 0.51	30
3	Green	0.53 - 0.59	30
4	Red	0.64 - 0.67	30
5	Near Infrared (NIR)	0.85 - 0.88	30
6	Shortwave Infrared (SWIR) 1	1.57 - 1.65	30
7	Shortwave Infrared (SWIR) 2	2.11 - 2.29	30
8	Panchromatic	0.50 - 0.68	15
9	Cirrus	1.36 - 1.38	30
10	Thermal Infrared (TIRS) 1	10.60 - 11.19	100
11	Thermal Infrared (TIRS) 2	11.50 - 12.51	100

Fig. 2. a) Study areas near Bruce Glacier, Treaty Glacier, Iron Cap, and Snow Field (indicated by black rectangles). **b)** Enlarged image of field sites near the Snow Field camp (in black polylines). Zone 9N, NAD 83.

105

Geological Fieldwork 2014, British Columbia Ministry of Energy and Mines, British Columbia Geological Survey Paper 2015-1

Fig. 3. Well-exposed altered rocks (silica-pyrite alteration) close to the Iron Cap camp (424998E, 626796N). Person (circled) for scale. Zone 9N, NAD 83.

processed for systematic radiometric and geometric correction using ground control points and the corresponding Digital Elevation Model (USGS, 2013c).

The Landsat 8 image used in this study (path 55 and row 20; Fig. 5) was captured on Aug. 3, 2013 under excellent
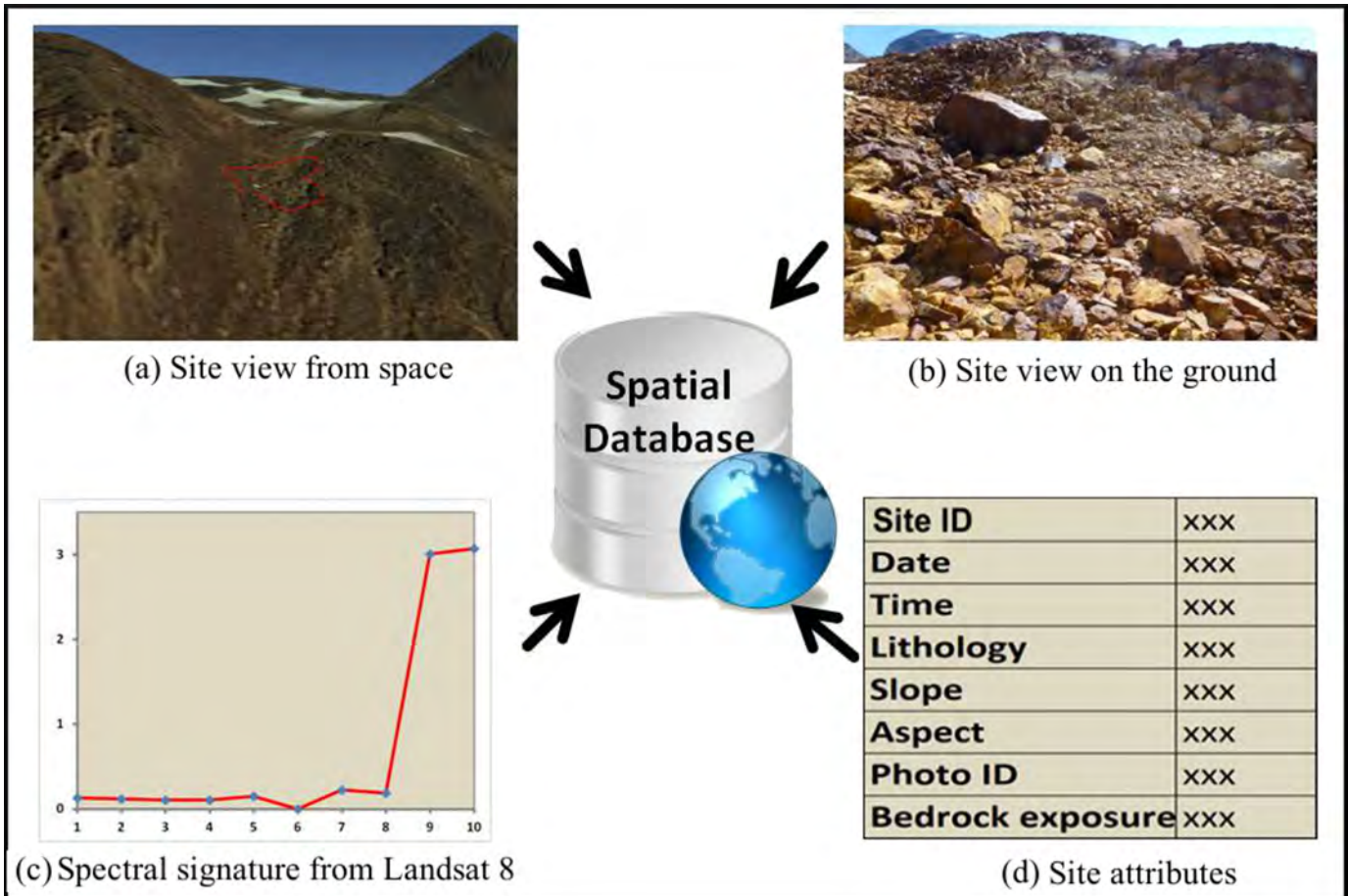
weather conditions (< 10% of cloud cover) while fieldwork was underway. The image was downloaded in a package containing 11 band images (in GeoTIFF), 1 quality assessment band image (in GeoTIFF), and 1 metadata file (in ASCII). Once the package was downloaded, the band images were processed as described below.

3.1. Spectral sub-setting

Because OLI band 8 (panchromatic) was designed for visualization and band 9 (cirrus) was for high-altitude cloud detection, they were excluded from further analysis. We created a nine-band image stack, including OLI bands 1 – 7 and TIRS bands 10 - 11 (Table 1).

3.2. Reflectance conversion

Level 1T images consist of Digital Numbers (DN) lacking physically meaningful units. They were converted to reflectance, representing the ratio of the radiation reflected off a surface to the radiation striking it. This conversion is commonly needed for quantitative remote sensing as it accounts for solar conditions (illumination, geometry, and intensity) when the images were acquired. The reflectance conversion was carried out using the method specified in USGS (2013e). Per pixel solar angles were used for more accurate reflectance

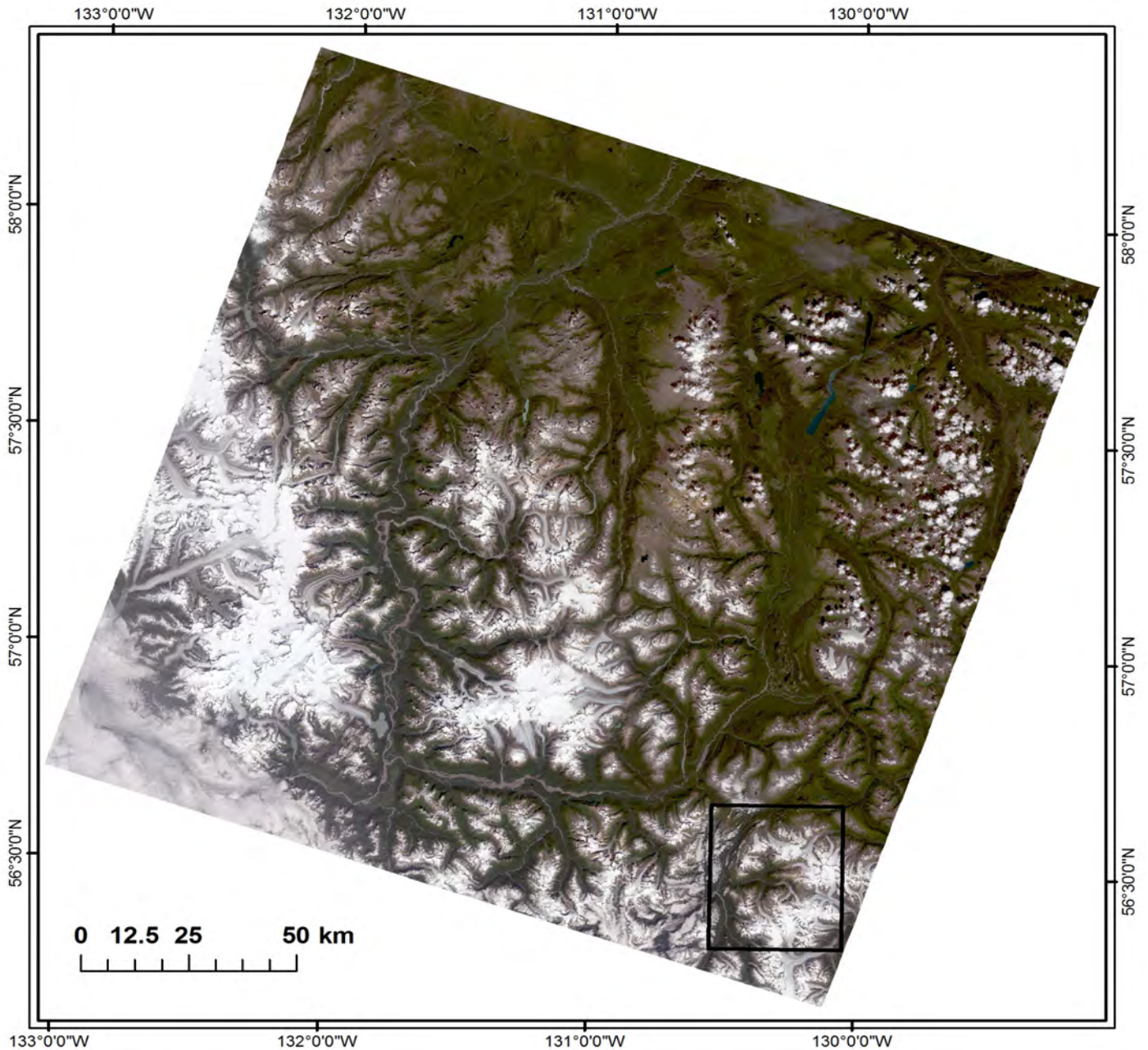**Fig. 4.** Conceptual model to develop spectral library for alteration mapping.

106

Geological Fieldwork 2014, British Columbia Ministry of Energy and Mines, British Columbia Geological Survey Paper 2015-1

Fig. 5. Landsat 8 level 1T image; study area indicated by black rectangle.

calculation. Because the interaction between solar radiation and gases and aerosols in the atmosphere is still included after the conversion, this step is more accurately called top of atmosphere (TOA) reflectance conversion. This interaction happens more prominently in bands with wavelengths shorter than 1000 nm. Similarly, the 2 TIRS bands were converted to at-satellite brightness temperature using the parameters and formula in USGS (2013d).

3.3. Masking

Because the bare Earth surface was the only land cover of interest in this study, materials (water bodies, ice, snow, cloud and shadow, and vegetation) were masked out from further image analysis. This masking was necessary to reduce image spectral variability arising from different land covers and to focus attention on the bare earth surface. The mask was created using information retrieved from the cirrus band, quality assessment band, and NDVI (Normalized Difference Vegetation Index) calculated using the TOA reflectance band images.

4. Image analysis

Incident solar radiation interacts with surface materials through electronic transitions, charge-transfers, and vibrational processes (Hunt, 1977). This interaction exhibits itself as absorption features (shown as dips in reflective spectral

107

Geological Fieldwork 2014, British Columbia Ministry of Energy and Mines, British Columbia Geological Survey Paper 2015-1

profiles) that extend across spectral ranges including visible and near infrared (VNIR), shortwave infrared (SWIR), and thermal infrared (TIR). Captured as images by remote sensing instruments, the reflected and emitted energy spectra can be used to identify those substances with diagnostic absorption features.

Some minerals and mineral assemblages in hydrothermally altered rocks have distinctive absorption features. For example, alunite and clay minerals such as illite, kaolinite, and montmorillonite have distinctive absorption features at ~2100 nm and their spectral responses peak at ~1700 nm (Sabins, 1999). Iron oxide and sulphate minerals commonly show low reflectance close to ultraviolet or blue but strong reflectance near red (Rencz, 1999), which gives them a rusty colour in a natural colour image. This observation led to the development of band-ratioing technique for visualizing hydrothermal altered rocks. For example, the ratio image of Landsat TM band 5 (1550 – 1750 nm) over band 7 (2090 – 2350 nm) is able to distinguish areas with high concentrations of alunite and clay, where pixels in the image appear bright. The radio image of band 3 (630 – 690 nm) over band 1 (450 – 515 nm) reveals areas where iron minerals are abundant (van der Meer, 2004).

Although the band-ratioing approach works reasonably well for visualization, it is inadequate for mapping, or other quantitative applications. The bandwidth assumed by optical multispectral remote sensing instruments is usually greater than 50 nm, which is too broad to unambiguously distinguish the individual spectral absorption features associated with specific alteration minerals. Also, many band-ratioing algorithms use only two or three bands even though multispectral images offer many more bands than that. Hence the image analysis approach we adopted in this study uses all nine bands together, taking advantage of the complete spectral information borne by the Landsat 8 image. As described below, feature extraction is the first step in this image analysis. This is followed by a spectral unmixing procedure to separate the spectra of altered rocks from other substances and derive a map for altered rock distribution.

4.1. Feature extraction

Between-band correlation is apparent among adjacent Landsat 8 band images, which degenerates the effectiveness of many image analysis methods, including the spectral unmixing employed in this study, which rely on image covariance matrix (Landgrebe, 2003). Feature extraction is a linear transformation that mitigates the correlation by projecting band images into a new space where the resultant images are orthogonal and arranged in terms of decreasing eigenvalues (representing information content) of the image covariance matrix. In this study, we used the Minimum Noise Fraction (MNF) for feature extraction.

4.2. Spectral unmixing

The Landsat 8 OLI band images have a spatial resolution

of 30 metres, and each pixel of an image covers an area of 900 m² (30 m x 30 m) on the ground. Generally, any given area of this size will be covered by different materials, referred to as endmembers, such as altered bedrock, unaltered bedrock, glacial till, gravel, and vegetation. Spectral unmixing is a method to determine the areal proportion occupied by such individual endmembers in each pixel. In this study, exposed altered rock is the endmember of interest. Altered rock spectra are extracted from the Landsat 8 image based on the GPS tracks collected during fieldwork. The endmember spectra of the exposed altered rocks are used as the 'knowns' in spectral unmixing, against which the Landsat 8 image pixel spectra, treated as the 'unknowns', are compared and unmixed.

4.3. Altered rock mapping

The result of the spectral unmixing is an image, called endmember abundance image, composed of pixels whose value represents the areal proportion (between 0 and 1) that a specific endmember occupies within that pixel. Brighter pixels in this image indicate areas where greater portions of the corresponding endmember occur. Using altered bedrock as the endmember, spectral unmixing generates an altered rock abundance image in which pixels with large proportions of altered rocks (> 0.6) are selected and labelled as the altered rock-dominated pixels. This image can then be used as a map to show the geographic distribution of the altered bedrocks across the entire Landsat 8 image.

4.4. Validation

Before accepting the generated altered rock abundance image, we validated the image using ground observations at altered rock sites. Because parts of these sites were used as the training data during the spectral unmixing process outlined above, we also checked the abundance image for altered rocks against the high-spatial resolution image offered through Microsoft Bing Web Map Service (WMS) where some highly altered rocks are visible.

5. Results and discussion

The effectiveness of the spectral unmixing described above depends on clearly distinguishing the spectra of altered bedrock from those of the other substances. Separating the altered rock spectra from those of water, snow, ice, and alpine vegetation is straightforward, because they have markedly different spectral shapes. Although separating altered and unaltered rocks is commonly more problematic, in some cases the distinction is clear. For example, outcrops of unaltered volcanic rock with local black lichen and patches of moss display spectra that differ from iron-stained, silica-clay-altered volcanic rock lacking vegetation (Fig. 6). Similarly, the spectra displayed by well-stratified, fine-grained siltstones and mudstones differ from clay-altered volcanic breccias (Fig. 7).

We further investigated spectral separation quantitatively using a spectral angle calculation (Clark et al., 1990). As there were 9 bands included in our image, each pixel spectrum
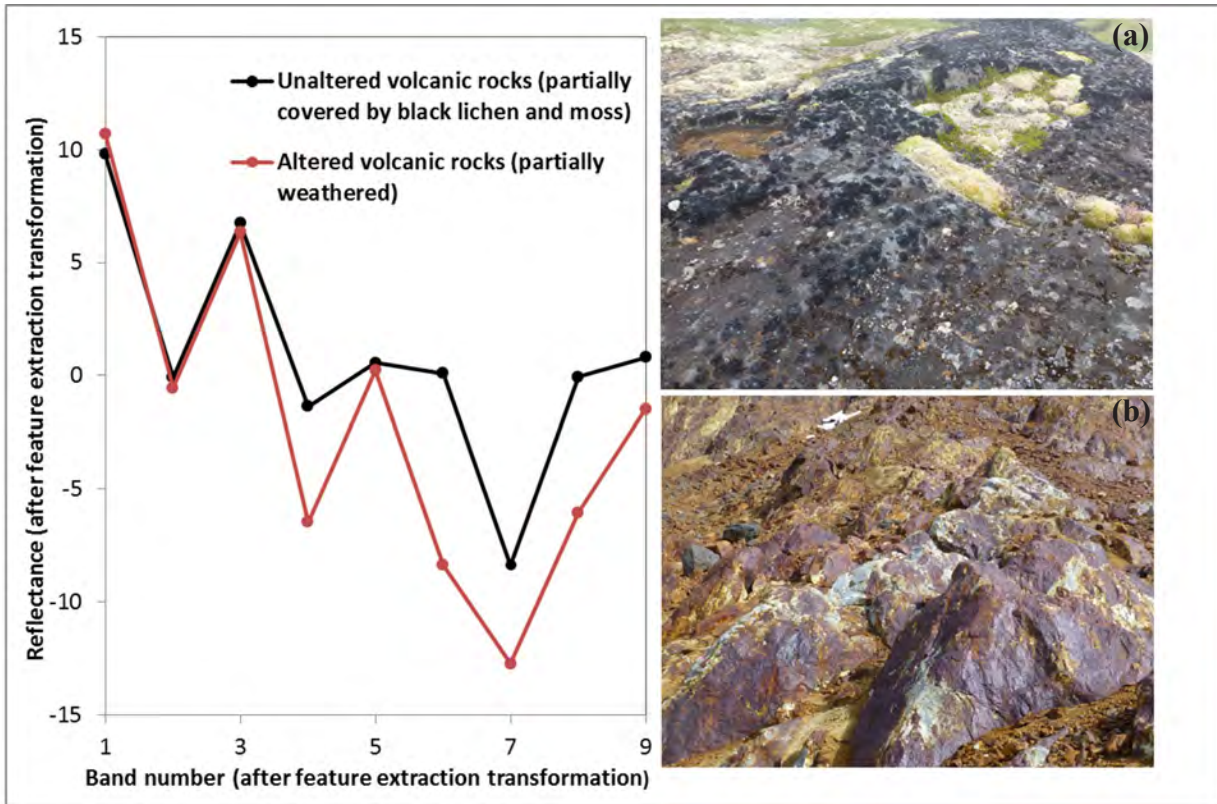
108

Geological Fieldwork 2014, British Columbia Ministry of Energy and Mines, British Columbia Geological Survey Paper 2015-1

Fig. 6. Spectral comparison between **a)** unaltered volcanic rocks (width of photo is ca. 50 m; centred at 413364E, 6270411N) and **b)** altered volcanic rocks (width of photo is ca. 60m; centred at 424979E, 6266848N). Zone 9N, NAD 83.
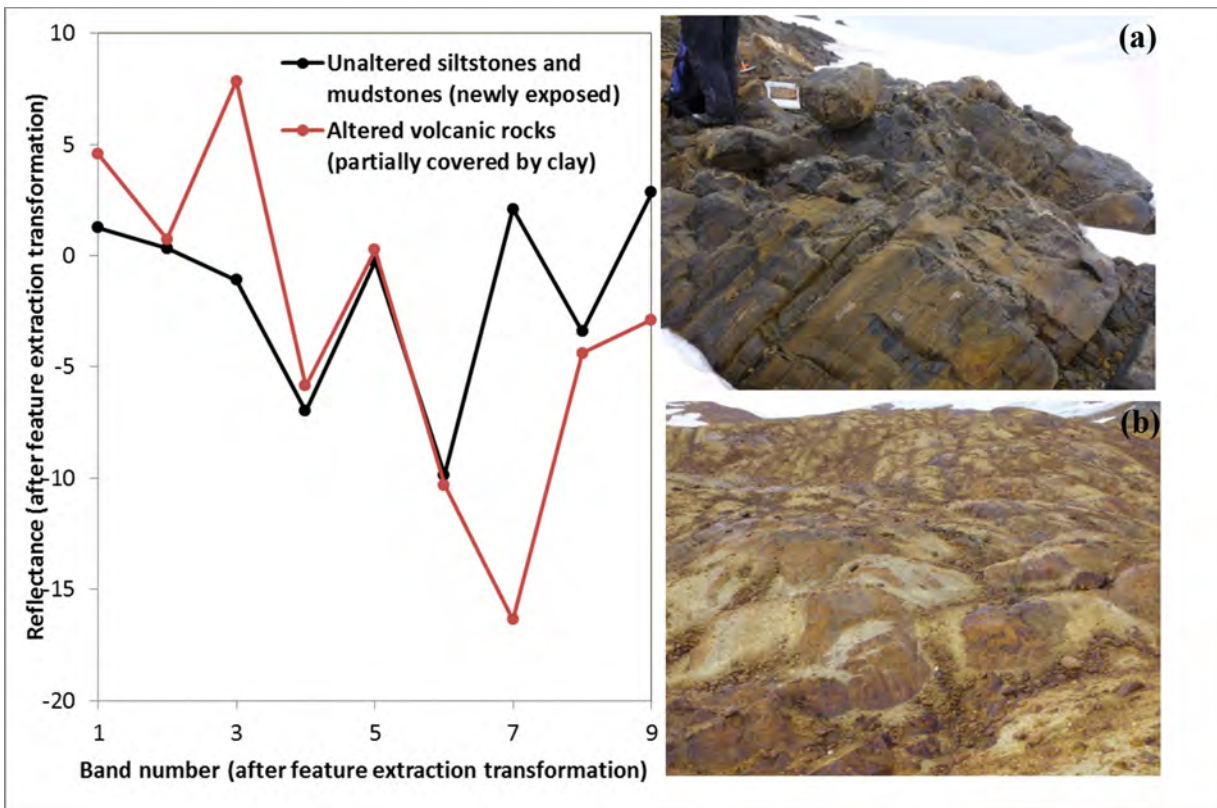

Fig. 7. Spectral comparison between **a)** unaltered fine-grained, well-stratified sedimentary rocks (width of photo is ca. 50 m; centred at 426939E, 6273494N) and **b)** altered volcanic rocks (width of photo is ca. 100m; centred at 424324E, 6264633N). Zone 9N, NAD 83.

109

Geological Fieldwork 2014, British Columbia Ministry of Energy and Mines, British Columbia Geological Survey Paper 2015-1

(extracted from the image) was considered as a vector in a 9-dimensional space. The spectral separability between any two pixel spectra was evaluated by calculating the angle (θ) between the two vectors (representing the two pixel spectra). The formula for θ is:

$$\theta = \cos^{-1}\left(\frac{a \cdot b}{|a||b|}\right)$$ where a and b are the two spectrum-representing vectors. Two groups of pixel spectra were assembled; one included 25 field sites of unaltered rocks and the other 43 sites of altered rocks. The average spectrum was calculated for each group and used as the endmember.

Using spectral angle calculation, we found that the angle between the two average spectra representing the altered and unaltered rocks is 17°, showing that the altered and unaltered spectra are separable at the group level. However, between-member spectral angles within each group varied considerably around its group average. The angle between the average spectrum of the altered rock group and each member spectrum ranges between 4 and 26°. For the unaltered rock group, the angle ranges between 7 and 28°. An angle overlap exists between the altered and unaltered rock spectra. These spectra are therefore not completely separable using only the spectral information derived from the Landsat 8 image; some altered rocks would be mistakenly identified as unaltered rocks and vice versa.

Considering the high relief of the study area, topography could be a factor that contributes significantly to the spectral response and shape of the altered and unaltered rocks, and may worsen the spectral separability (Gitas and Riano et al., 2003; Devereux, 2006). For this reason, slope and aspect images derived from the TRIM DEM (GeoBC, 2014) were brought in as additional information to characterize the terrain and to assist the spectral unmixing operation. The 43 altered field sites were assigned to eight categories (Table 2) based on their slope and aspect. The average spectrum was calculated within each category and designated as the endmember spectrum with the specific slope and aspect values. The spectral angle between the average spectrum and each member spectrum within each category was then recalculated. The range of angles across all categories (between 4 and 19°), is significantly narrower than the range without topographic categorization (between 4 and 26°). Taking into account the topographic factors of slope and aspect helped to separate the altered and unaltered rock spectra.

Upon spectral unmixing, the slope and aspect of each pixel

Table 2. Field site categories by slope and aspect (the compass direction that a slope faces).

Category	Slope (degree)	Aspect (degree)
1	0 - 20	0 - 89
2	21 - 45	0 - 89
3	0 - 20	90 - 179
4	21 - 45	90 - 179
5	0 - 20	180 - 269
6	21 - 45	180 - 269
7	0 - 20	270 - 359
8	21 - 45	270 - 359

being unmixed were read out first, which was followed by selecting the endmember (altered rock) spectrum in the same slope and aspect category. Both the spectrum of the pixel being unmixed and the endmember spectrum were fed into the unmixing process. This gave rise to a topographic decision-assisted spectral unmixing method, where the decision was made based on pixel's slope and aspect. Following through the entire process of image processing and analysis, a map was generated outlining areas of significant alteration, which was rendered on top of a high-resolution Microsoft Bing WMS image (Fig. 8).

We verified our alteration map with ground observations from 100 field sites. Ground and remotely sensed observations agreed at 83 of the sites, but 17 sites where altered rocks are exposed were misidentified as containing unaltered rocks. The misidentified sites have either weak surficial expression of alteration or exposure that covered only a small part of an image pixel. As further verification, the alteration zones identified by the Landsat-8 data correspond well with colour anomalies recording red to orange gossans on the Microsoft Bing WMS image (Fig. 8b).
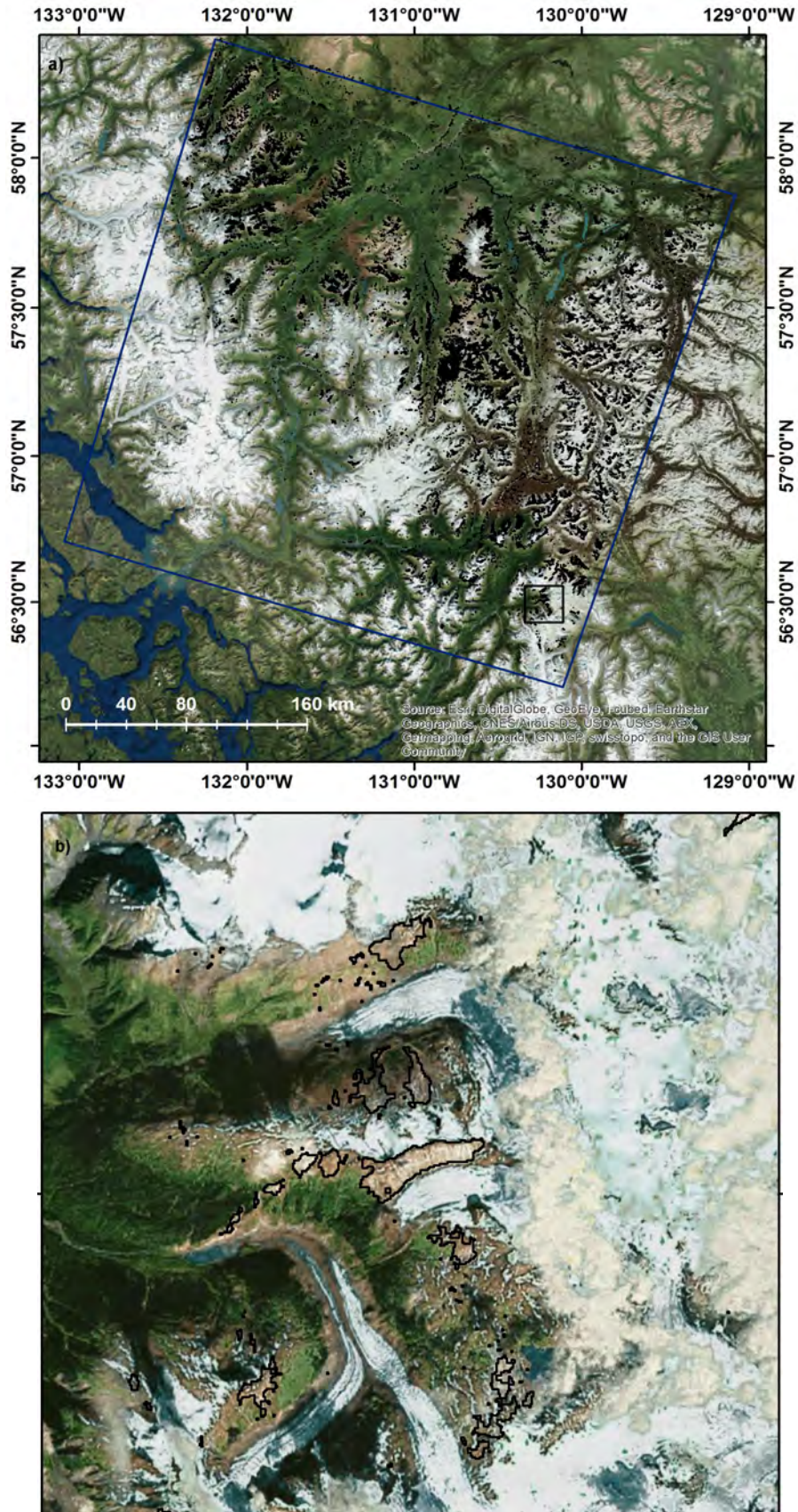
6. Conclusions and further work

This trial study demonstrates that analysis of a Landsat 8 image based on spectral unmixing can be effective for mapping hydrothermally altered rocks. This method was able to address the influence of topography on the surface spectral response, an important consideration in high-relief terrains such as the Cordillera. Including topographic factors in spectral unmixing helped distinguish altered and unaltered rock spectra, which helped produce a more accurate map.
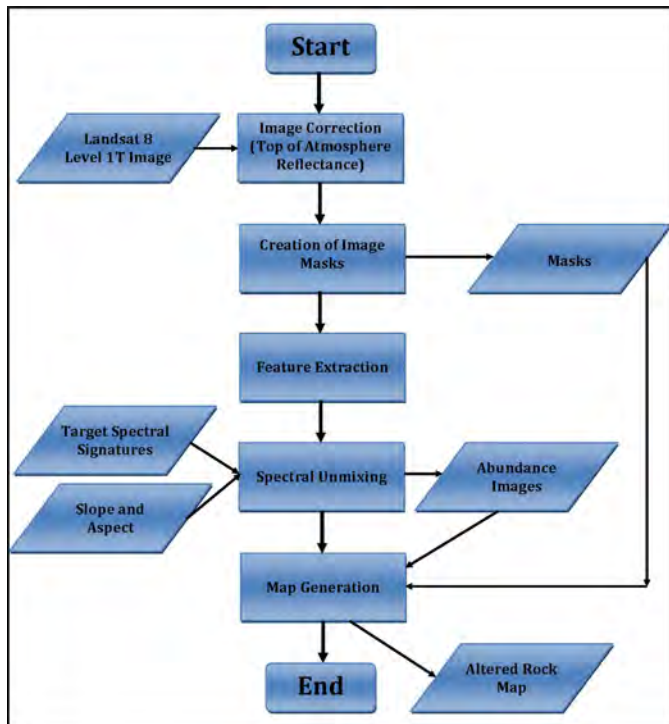
Image processing and analysis for alteration mapping include several steps that can be streamlined by a semi-automated process (Fig. 9). Because a single Landsat 8 image covers an area with dimensions of ~183 x 170 km, this method has the potential to quickly and inexpensively identify areas of altered rock and guide regional mineral exploration. The method may be of particular value in remote, recently deglaciated regions of northwestern British Columbia.

Future work might aim at collecting more detailed field data to enhance the spectral library, including rock spectra from the field, rock surface roughness, percentage of bedrock exposure, and topography. These data are vital to characterize the altered and unaltered rocks and to better separate their pixel spectra. Because the Landsat 8 image used in this study was only corrected to the top of atmospheric reflectance, atmospheric contaminations remain in the image, which may blur the spectral boundary between the altered and unaltered rocks. Pixel-based full atmospheric correction is preferred for further work.

Landsat 8 has a 30-metre spatial resolution and ~50-nm spectral resolution for its OLI channels. These resolutions may be sufficient for regional work, but are inadequate for property-scale mapping. Using images with the higher spatial and spectral resolutions, such as those acquired by Worldview 3

110

Geological Fieldwork 2014, British Columbia Ministry of Energy and Mines, British Columbia Geological Survey Paper 2015-1

Fig. 8. a) Altered rock (in black) distribution plotted on Microsoft Bing WMS image. Blue rectangle marks the area of Landsat 8 image used in this study. **b)** Landsat 8 image mapped altered rocks (in black polylines) indicated by the black rectangle in a).

111

Geological Fieldwork 2014, British Columbia Ministry of Energy and Mines, British Columbia Geological Survey Paper 2015-1

Fig. 9. Landsat 8 image processing and analysis for alteration mapping.

(Kruse and Perry, 2013) or airborne platforms, may be more appropriate for property-scale work, because they have the capacity to map not only altered rocks but hydrothermal mineral assemblages or even individual minerals. Potentially, property-scale image-based multispectral alteration maps could be used in conjunction with core spectrometer logs to create three-dimensional alteration mineral zoning models.

References cited

Clark, R.N., King, T.V.V., Kleijwa, M., Swayze, G.A. and Vergo, N., 1990. High spectral resolution reflectance spectroscopy of minerals. Journal of Geophysical Research, 95, 12653–12680.

Gabr, S., Ghulam, A., and Kusky, T. 2010. Detecting areas of high-potential gold mineralization using ASTER data. Ore Geology Reviews, 38, 59-69.

GeoBC, TRIM Program, http://geobc.gov.bc.ca/base-mapping/atlas/trim/. Accessed: July 14, 2014.

Gitas, I.Z., and Devereux, B.J., 2006. The role of topographic correction in mapping recently burned Mediterranean forest areas from Landsat TM images. International Journal of Remote Sensing, 27, 41 – 54.

Hunt, G.R. 1977. Spectral signatures of particulate minerals, in the visible and near-infrared. Geophysics, 42, 501-513.

Irons, J. R., Dwyer, J. L., and Barsi, J. A., 2012. The next Landsat satellite: The Landsat data continuity mission. Remote Sensing of Environment, 122, 11–21.

Kruse, F. A., and Perry, S. L., 2013. Mineral mapping using simulated Worldview-3 short-wave-infrared imagery. Remote Sensing, 5, 2688 – 2703.

Landgrebe, D.A., 2003. Signal theory methods in multispectral remote sensing, John Wiley & Sons, Inc. New Jersey, 323p.

Loughlin, W.P., 1991. Principal component analysis for alteration mapping. Photogrammetric Engineering & Remote Sensing, 57, 1161–1169.

Mars, J.C., and Rowan, L.C., 2006. Regional mapping of phyllic- and argillic-altered rocks in the Zagros magmatic arc, Iran, using Advanced Spaceborne Thermal Emission and Reflection Radiometer (ASTER) data and logical operator algorithms. Geosphere, 2, 161-186.

Nelson, J., and Kyba, J. 2014. Structural and stratigraphic control of porphyry and related mineralization in the Treaty Glacier – KSM – Brucejack – Steward trend of western Stikinia. In: Geological Fieldwork 2014, British Columbia Ministry of Energy and Mines, British Columbia Geological Survey Paper 2014-1, pp. 111-140.

Rencz, A. N. 1999. Manual of remote sensing: Remote sensing for the earth sciences, John Wiley & Sons, 47p.

Riano, D., E. Salas, C, J., and Aguado, I., 2003. Assessment of different topographic corrections in Landsat-TM data for mapping vegetation types, IEEE Transactions on Geoscience and Remote Sensing, 4, 1056–1061.

Rowan, L.C., Wetlaufer, P.H., Goetz, A.F.H., Billingsley, F.C., and Stewart, J.H. 1974. Discrimination of rock types and detection of hydrothermally altered areas in south central Nevada by the use of computer-enhanced ERTS images. USGS Professional Paper, 883, 35p.

Sabins, F. F., 1999. Remote sensing for mineral exploration. Ore Geology Reviews, 14, 157–183.

USGS, 2013a. Frequently asked questions about Landsat missions: http://landsat.usgs.gov/band_designations_landsat_satellites.php Accessed Aug. 22, 2014.

USGS, 2013b. Earth Explorer: http://earthexplorer.usgs.gov/ Accessed Aug. 20, 2014.

USGS, 2013c. Landsat 8 data products: http://landsat.usgs.gov/landsat8.php, last access: Aug. 20, 2014.

USGS, 2013d. Using the USGS Landsat 8 Product: http://landsat.usgs.gov/Landsat8_Using_Product.php Accessed Aug. 20, 2014.

van der Meer, D. F. 2004. Analysis of spectral absorption features in hyperspectral imagery. International Journal of Applied Earth Observation and Geoinformation, 5, 55 – 68.

van der Meer, D. F., Harald, M. A., van der Werff, F. J. A., van Ruitenbeek, C. A., Hecker,, W. H., Bakker, M. F., Noomen, M., van der Meijde, E., Carranza, J. M., Boudewijn de Smeth, J., and Woldai, T., 2012. Multi- and hyperspectral geologic remote sensing: A review. International Journal of Applied Earth Observation and Geoinformation, 14, 112 – 128.

112

Geological Fieldwork 2014, British Columbia Ministry of Energy and Mines, British Columbia Geological Survey Paper 2015-1